Electro-Optical Imaging Microscopy of Dye-Doped Artificial Lipidic Membranes

Bassam Hajj, Sophie de Reguardati, Loic Hugonin, Bruno Le Pioufle, Toshihisa Osaki, Hiroaki Suzuki, Shoji Takeuchi, Halina Mojzisova, Dominique Chauvat, Joseph Zyss

Electro-Optical Imaging Microscopy of Dye-Doped Artificial Lipidic Membrane

Bassam HAJJ [*], Sophie DE REGUARDATI [†], Loïc HUGONIN [†], Bruno LE PIOUFLE [†], Toshihisa OSAKI [‡], Hiroaki SUZUKI [‡], Shoji TAKEUCHI [‡], Halina MOJZISOVA [*], Dominique CHAUVAT [*], Joseph ZYSS [*].

[*] *Laboratoire de Photonique Quantique et Moléculaire, d'Alembert Institute, ENS Cachan, 61 avenue du Président Wilson, 94235 Cachan, Cedex, France Centre National de la Recherche Scientifique (UMR8537)*

[†] *Systèmes et Applications des Technologies de l'Information et de l'Energie, d'Alembert Institute, ENS Cachan, 61 avenue du Président Wilson, 94235 Cachan, Cedex, France Centre National de la Recherche Scientifique (UMR8029)*

[‡] *Center for International Research on Micro Mechatronics, Institute of Industrial Science, University of Tokyo, 4-6-1 Komaba, Meguro-ku, Tokyo 153-8505 Japan*

Abstract:

Artificial lipidic bilayers are widely used as a model for the lipid matrix in biological cell membranes. We use the Pockels electro-optical effect to investigate the properties of an artificial lipidic membrane doped with nonlinear molecules into the outer layer. We report here what is believed to be the first electro-optical Pockels signal and image from such a membrane. The electro-optical dephasing distribution within the membrane is imaged and the signal shown to be linear as a function of the applied voltage. A theoretical analysis taking into account the orientation distribution of the inserted dye molecules allows to estimate the doped membrane nonlinearity. Future extensions of this work to living cell membranes are discussed.

1. Introduction:

As the main component of cellular membranes, lipid bilayers play an essential role as a barrier protecting the cell and its intracellular organelles. The cellular membranes also maintain the solute and ion concentration gradients which induce the equilibrium transmembrane potential. In the case of excitable cells, the plasma membrane ensures the propagation of the action potential.

Various experimental techniques have been used in cellular electrophysiology for stimulation and measurement of membrane potentials by use of intracellular electrodes(1-2), which has lead to the well known patch-clamp technique (3). Although these techniques are extremely sensitive and allow to record the electrical activity down to a single ion channel, they lead to cell death and provide the information about the potential in a single location within one neuron. Optical approaches using light scattering and intrinsic birefringence changes were investigated (4-5). Voltage-sensitive amphiphilic dyes were introduced to enhance the latter effect (6), and were found to show voltage-dependent change in absorption, dichroism (7), and fluorescence (8-9). Such electrometric dyes bind to the external cell membranes and contain an electron donor-acceptor group leading to electrochromism and a high hyperpolarizability. The membrane depolarization and the action potential propagation can then be recorded at different points of the cell as a voltage-induced fluorescence variation (10-12), or by nonlinear microscopy techniques, in particular by second-harmonic generation (SHG) (13-15). Voltage-induced SHG is a third-order nonlinear process described by an effective rank-four nonlinear susceptibility tensor associated to both quadratic and cubic time-dependent molecular hyperpolarizability tensors. The former is underlying field induced orientational effects and the latter instantaneous four-wave mixing. Therefore SHG-based membrane potential measurements monitor the electrically induced changes of hyperpolarizability and/or the alignment of the dye molecules in the bilayer (14-15). A major interest of nonlinear microscopy lies in its intrinsic three-dimensional sectioning capability related to the two-photon excitation step that occurs mainly in the focal volume together with the low photobleaching of out-of-focus molecules. It should be however noted that the bleaching may be increased in the focal spot due to the use of pulsed femtosecond lasers. Remarkably, the non-centrosymmetric organization of the dye molecules, inserted exclusively into the external membrane layer and responsible for SHG, is also at the origin of the related electro-optical Pockels effect (16). The Pockels effect is a variation of the index of refraction Δn induced by a quasi-static applied electric field. When probed by a laser beam, Δn induces an optical phase shift which can be detected with an interferometric setup. Since the Pockels effect is a non-resonant process, it can be measured using a low-power continuous wave laser, which preserves the integrity of the sample, and more generally avoids the use of costly and cumbersome high power short pulse lasers.

In this work we present an original electro-optical microscopy study of the variation of membrane potential in model lipid bilayers stained by the potentiometric Di-8-ANEPPS dye. We measure the absolute change in index of refraction due to electro-optical effect along a chosen polarization axis. Since lipid bilayers are considered to be an adequate model for the investigation of the electric properties of biologic membranes (17), electro-optical measurements were subsequently performed on a phosphatidylcholine bilayer formed on a parylene biochip. Our results demonstrate the imaging capability of an advanced electro-optical microscope in a microfluidic environment suitable for biology-related studies.

2. Principle and theory:

The electro-optical (EO) effect of a non-centrosymmetric material, or Pockels effect, is the change of the index of refraction of this medium in response to a quasi-static electrical field

applied using adequately shaped electrodes (18). The index of refraction change can be read out as an additional small phase shift on a probing light wave. While the Pockels effect stems from a second-order (rank three) nonlinearity, it can also be viewed as a linear optical response in the electric field of the probe light field E_{op}, which also depends linearly on the applied external quasi-static electrical field E_S.
The index of refraction change along the *i* axis is given by

$$\Delta \mathbf{n_i} = \frac{\mathbf{n_i^3}}{2} \sum_j \boldsymbol{r_{ij} E_j} \ , \quad \textbf{(1)}$$

where E_j is the component of the applied electric field E_S in the *j* direction (See Appendix A). The proportionality factors r_{ij} are the coefficients of the electro-optical tensor (18). We choose {x,y,z} as the principal axes of the nonlinear material, i.e., perpendicular to the plane of the doped bilayer (see Fig. 1). z is along the applied field direction and x,y are arbitrary directions in the sample plane.
Depending on the orientation of the molecules inside the medium and the associated geometrical symmetry, some r_{ij} coefficients cancel and some are related one to the other. In the case of an artificial bilayer doped with an ensemble of dye molecules, the cylindrical symmetry around the z axis leads to the following tensor (see Appendix A)

$$[\boldsymbol{r_{ij}}] = \begin{pmatrix} \mathbf{0} & \mathbf{0} & \boldsymbol{r_{13}} \\ \mathbf{0} & \mathbf{0} & \boldsymbol{r_{13}} \\ \mathbf{0} & \mathbf{0} & \boldsymbol{r_{33}} \\ \mathbf{0} & \boldsymbol{r_{13}} & \mathbf{0} \\ \boldsymbol{r_{13}} & \mathbf{0} & \mathbf{0} \\ \mathbf{0} & \mathbf{0} & \mathbf{0} \end{pmatrix} . \quad \textbf{(2)}$$

In this notation index '3' is related to the z direction of propagation of the light, perpendicular to the bi-membrane (see Fig. 1).
The induced EO phase shift is

$$\boldsymbol{\Delta\varphi_i} = \frac{\boldsymbol{2\pi}}{\boldsymbol{\lambda}} \boldsymbol{e \Delta n_i} \ , \quad \textbf{(3)}$$

that can be developed as

$$\boldsymbol{\Delta\varphi_i} = -\frac{\boldsymbol{\pi}}{\boldsymbol{\lambda}} \boldsymbol{e n_i^3} \sum_j \boldsymbol{r_{ij}} \boldsymbol{E_j} \ . \quad \textbf{(4)}$$

A signature of the effect can be obtained by rotating the polarization of the linearly polarized incident light. Inspection of the electro-optical tensor matrix shows that the phase shift must not change when the polarization of the incident beam is rotated within the (x,y) plane of the sample, as it involves the same r_{13} EO coefficient, in agreement with the cylindrical symmetry about the z axis. We therefore note that a polarimetric detection setup with crossed polarizer and analyser, which is sensitive to a differential phase shift between two orthogonal directions, would not detect the above isotropic phase shift.
An optical scheme capable of measuring the absolute EO phase shift along one given polarization direction is thus required. Such scheme could measure the electrical field $\overrightarrow{E_s}$ if the EO coefficients are known, or conversely the EO coefficients can be extracted when the electric field $\vec{E}$ is known. If both are undefined, it can access to the $E_j\ r_{ij}$ product.
Assuming a potential of 10mV throughout a membrane of e=7nm thickness and a realistic *r* coefficient of the order of 1pm/V for a doped membrane, one should be able to measure a corresponding phase shift variation $\Delta\varphi$ of the order of 10^{-7} radian.
In order to measure this additional EO dephasing contribution, we use an interferometric scheme described below.

3. Sample and optical methods:

3.a Electro-optic microscope:

The principle of measuring an electro-optical phase shift is shown in Fig. 2. A continuous wave He-Ne laser is used as the source of light, its beam being subsequently separated in two.

One part is focused on the doped lipidic membrane through a microscope objective (Nikon , CFI plan-fluor 40× , N.A. = 0.6), then transmitted and collected via an identical microscope objective in forward direction. It is then recombined with the other beam that plays the role of the reference arm in a Mach-Zehnder interferometric scheme (19). The interference optical signal is detected by two photodiodes (Hamamatsu). The electric field applied on the sample is typically modulated at a frequency $\Omega = 20$ kHz, inducing a modulated phase shift and interference fringes changes at the same frequency. To reach a high sensitivity for detecting a small phase shift variation, a balanced homodyne detection based on two photodiodes is being used (20). A lock-in amplifier (EG&G Princeton Applied Research, Model 5302) is used to measure this modulated phase shift with high signal-to-noise ratio. The sensitivity of the interferometric detection to the EO phase shift is maximized if the static optical path difference between the two beams corresponds to a phase shift $\varphi_{OL} = \pi/2$ rad. A phase control loop is therefore implemented in the system, with a mirror mounted on a piezo-electrical transducer stage (PI ceramic). It is added to the optical path of the reference beam and its translation allows to change the quasi-static optical path length (not shown in Fig. 2).
Let us note that in principle an electrically-induced absorption modification would also lead to a signal modulated at frequency Ω. However, with the above phase working point $\varphi_{OL} = \pi/2$, the lock-in amplifier is sensitive only to the EO phase-shift, while $\varphi_{OL} = 0$ would render the detection system sensitive to a modulated absorption (See Appendix C).
Two half-wave plates (Fichou, France) allow to control the polarization of the light focused onto the sample.

3.b Sample composition and fabrication:

Bio chip:

As a sample holder, we use a home-made bio-chip made of parylene. It is encapsulated in a resist that has been photopatterned in three dimensions thanks to a stereolithography process (21). The parylene thin film of 20µm thickness was micromachined using O_2 plasma in reactive-ion-etching through an aluminum mask, which leads to an array of trough holes devoted to the bilayer reconstruction. In each microchamber, 9 holes of diameter 40 µm allowed the simultaneous formation of 9 bilayers (22-24).

Electrodes:

Two Ag/AgCl electrodes, connected to the solutions from each side of the bilayer, were used to apply a voltage difference. The coating of silver electrodes is deposited by dipping the electrodes for a few minutes in a nitric and hydrochloric acid (ROTH) (1/3 vol.vol) concentrated solution. By dipping the electrodes in this bath for a few minutes, we obtained a pure, thin and uniform chloride silver coating.

3.c Mechanism of bilayer formation:

Prior to this experiment, the bio-chip is first put into an ultra-sound bath in ethanol solution for 5 minutes, and then in another ultra-sound bath in Millipore water solution for 2 minutes. It was rinsed with Millipore water, dried with compressed nitrogen, then in an oven (40°C, 10mn).
15µl of a buffer solution of KCl 0.1M (Fisher Scientific) and MOPS (*3-(N-morpholino)propanesulfonic acid)* 10mM pH7 (Research Organics) was inserted in the upper chamber (see Fig. 3.a). The lipid used was L-α-phosphatidylcholine (Egg, Chicken) (Avanti Polar Lipids), 20 mg/ml dissolved in N-decane (Merck). 8µl of the lipid solution was flowed in the lower channels (see Fig. 3.b), followed by the flowing of buffer, which permits the formation of the bilayers (see Fig. 3.c), as described in Refs. (21-22).

Staining of the bilayer:

To generate an electro-optical phase shift the medium has to display a non-centrosymmetric statistical arrangement. The lipid molecule by itself satisfied this condition, but in the case of a bilayer the head-tail molecular assembly leads to a centrosymmetric system, and subsequent cancellation of the EO effect. In order to confer electro-optical activity to the membrane we asymmetrically stained the membrane with a non-centrosymmetric probe molecule Di-8-ANEPPS (Invitrogen). This molecule has a long carbon chain, thus adequately lengthening the flip time across the membrane (9,25). Those properties make Di-8-ANEPPS a dye that has been widely used for fluorescence or SHG measurement of membranes (26-27), and as an electrical potential probe (9,12,25,28-32). Its orientation in the membrane was investigated (27,33), and different models were proposed.
The stock solution was prepared in DMSO (Sigma Aldrich) at 1mg/ml concentration. 3µl of the dye was introduced to the upper chamber already filled with the buffer just after the injection of the lipid in the lower channel. Then a glass plate was placed on the bio-chip to cover the upper chamber. It was used to prevent the formation of a curved liquid surface that could act as a micro-lens and thus affect the probe laser beam that passes through it. The glass plate was perforated to insert an electrode inside the buffer solution. Then, as explained above the buffer was introduced in the lower channel and the bilayer formed. A 15-minute waiting time between the introduction of the dye and the start of the measurement allowed the dye to intercalate into the upper layer of the artificial bilayer.
In order to check that the lipidic membrane was organized as a bilayer, a capacitance measurement between both sides of the membrane was made before and after the electro-optical measurement described below. The same capacitance 0.32 $\mu F/cm^2$ measured at the beginning of the experiment was found also at the end. This is in good agreement with the values of surface capacitance of bilayers (0.4 $\mu F/cm^2$) reported in the literature (34).

4. Results:

Once a stable bilayer was formed in the bio-chip, we were able to stain the membrane and then perform the electro-optical measurement. The dye was inserted on one side of the lipidic membrane, and a modulated electric field was applied between both sides of this membrane. A sinusoidally-varying potential difference up to 10 Volts maximum amplitude was applied to the membrane without breaking it, and its electro-optical response was registered.
The modulated electric field induced a modulated phase shift in the laser beam that probes the EO active sample. Though the signal was small, our interferometric setup proved sensitive enough for measuring this electro-optical phase shift through the membrane.
First the electro-optical signal was detected with a good signal-to-noise ratio (SNR). For a voltage difference of 5V peak-to-peak amplitude at 100 kHz, the SNR was 10 ± 1 for 20 ms integration time. Second we observed that the temporal response of the system was fluctuating (Fig. 4). This may be due to impurities inside the buffer passing through the probe beam during the measurement.
The frequency of the modulated electric field applied to the membrane is limited by the cut-off frequency of the whole system. The bilayer and the surrounding buffer can be modeled as a capacitor and a resistance (35). We estimate a cut-off frequency about 3 MHz, well above the frequency used for the measurement. As for the conductivity of the buffer necessary to transfer the voltage difference to the membrane at a given frequency, we calculated a cut-off frequency of 260 MHz.
In order to check the origin of the detected signal, we changed the amplitude of the applied potential difference. Temporal signal of the lock-in amplifier was recorded for each modulated voltage amplitude, and the dependence of the EO signal on the applied voltage was plotted. Fig. 5 shows a linear dependence, as expected for the Pockels effect (from Eq.1).

From the slope of this curve we could extract the electro-optical coefficient of the membrane. The slope $\Delta\varphi/E$ is (43.8 ± 1.7) $\times 10^{-6}$ rad/V, which is theoretically equal to $\frac{\pi}{\lambda} e n^3 r_{13}$ (see Eq. 18 in Appendix). The laser wavelength λ is 632.8 nm. It is difficult to give accurate values to the thickness and index of refraction of the membrane for the electro-optical response. Here we make the assumption that a macroscopic description of this ultra-thin optical device is valid, which is commonly done for thin films (10). Under this assumption, e=7nm and n≈1.5 seem to be safe values, which have been used in the literature (36). Then one can estimate the membrane EO coefficient r_{13} =2.6 pm/V. This value seems reasonable since it can lead to non-negligible SHG signals as those reported in ref (27).

Fig. 6 shows a typical raster scan of a membrane under a 5V peak-to-peak sinusoidal voltage at 20 kHz frequency. The contour of the hole holding the membrane can be distinguished. The signal is higher at the center of the membrane, maybe due to a higher density of Di-8-ANEPPS molecules at the center of the hole, itself due to a possible Gibbs plateau on the circumference of the hole. The inset on Fig. 6 shows another scan during which the membrane was broken.

In order to test the symmetry of the dye orientation distribution, the linear polarization of the incoming light was switched perpendicular to the previous one, i.e, from x to y axis in Fig. 1. The results are given in Tab. 1. The signal did not change within 2%, as expected from the cylindrical symmetry about the z axis (see Fig. 1), hence the same electro-optical coefficient is found in both configurations. Again we note that this isotropic phase shift distribution of the EO variation of the index of refraction could not be detected by a standard polarimetric setup sensitive to birefringence.

We compared such a response to a home-made reference sample built with a $LiNbO_3$ single crystal plate (see Tab.1). This reference is highly anisotropic in its x and y responses, which confirmed the polarization sensitivity of our interferometric detection method. Therefore any change of dye alignment in the membrane can be readily detected by our set-up.

5. Discussion and Conclusion:

In conclusion we demonstrated that the electro-optical effect can be used to quantitatively image a dye-doped artificial membrane. We checked that the EO response is proportional to the applied voltage difference as expected for the Pockels effect. Using different optical polarization, we also checked the symmetry of the doped membrane around the direction normal to the bilayer, and proved that this microscopy is able to probe the statistical orientation order of the dye inside the membrane. We point out that this interferometer is sensitive to absolute electro-optical variation of the index of refraction along one selected polarization direction. Estimating the applied electrical field we obtained a reasonable value for the dye-doped membrane nonlinear susceptibility $r_{13} \approx 2.6$ =2.6pm/V. If the nonlinear susceptibility is known independently, for instance from SHG measurement, our method provides a non-resonant optical measurement of the transmembrane potential. This second approach therefore allows to investigate electrical fields in doped lipid membrane.

We note that the above results rely on average values over the membrane. A future analysis taking into account the distribution of the field and exact molecular insertion could be performed by using different dye molecules. At the scale of a single layer of molecules, we may also observe heterogenous physical effects, in terms of thin-film organization and for multicomponent membranes which will require a refined model.

We note that a modulated sinusoidal potential difference of 1 Volt amplitude at a relatively high frequency varied from 15 to 100 kHz, was not invasive to the membrane. For an unstained membrane the voltage reached 4 Vpp at frequency = 20 kHz before breaking the membrane, in the case of an electrical capacitance of 33 pF for 9 simultaneous bilayers. With

stained lipidic membranes, some of them could withstand a voltage application up to 20Vpp at 20 kHz, without damage. This observation is quite surprising since it is well known that when a DC potential difference higher than 1V is applied to a bilayer, it is depolarized by the corresponding static electric field and the membrane is broken (37-39). The enhanced robustness of the membrane to higher voltage is probably linked to the sinusoidal character of the potential difference. This unexpected result has to be investigated in future work.

Many developments of the technique can now be envisioned. For instance, in order to fully characterize the orientation order of the dye in the artificial bilayer (see Fig. 7), the average tilt angle $\langle\theta_0\rangle$ of the molecule being given by the coefficient ratio $r_{13}/r_{33} = \langle tan\,(\theta_0)\rangle/2$ (see Appendix Eq.15), a light polarization in the z axis direction could be applied on the membrane by focusing an inhomogeneously polarized beam (40). Furthermore new bio-chips where the flow of buffer solution in the upper chamber may be modified can also be designed. It would allow us to change the dye concentration during a single experimental measurement and also to insert membrane proteins that have the potential to control membrane channel opening and the related ionic concentration that are responsible for membrane potential variations.

Finally, it can also be envisioned to probe the depolarization of plasma membrane after stimulation and in long term the propagation of an action potential in an excitable cell. Some bottlenecks have however to be considered. First, such internally generated electrical field is a self-triggered train of pulses rather than a sine wave at a definite frequency. Therefore a new asynchronous detection technique has to be developed. The pulse repetition rate being also low, an heterodyne detection would be a good candidate to shift low frequency to a higher noise-less one (41). Second, in the case of a living cell the surface is not flat thus leading to a tilt angle α of the normal direction to the membrane with respect to the microscope Z-axis at the probe beam position (see Fig. 8). In this case new electro-optical coefficients will appear (see Appendix C Eq. 22). A simultaneous polarization measurement in two perpendicular polarizations could measure this local tilt α. Third, for thick biological sample a transmission mode clearly constitute a limitation. A reflection one could be used since the index of refraction variation under an applied electric field induces a variation of the reflection coefficient of the membrane. Using Abeles matrix in stratified medium (19), the expected intensity reflection coefficient is approximately 10^{-5} in intensity, and the electro-optical contribution is estimated to be $\approx 2 \times 10^{-8}$.A modified setup with enhanced sensitivity is envisioned to detect this small effect.

While the ultimate goal of applying our technique to the electrical activity of a living cell, under investigation in our lab, is challenging, the results presented here are promising to further explore an all-optical patch-clamp technique.

6. Acknowledgments:

We thank Jean-Pierre Lefèvre and Jean-Pierre Madrange for technique assistance. We acknowledge contract CNano MELOA and F-I Bio-imaging. B.H. thanks CNRS for PhD grant. L.H. and T.O. recognize CNRS for post-doctoral grant. H.M. acknowledges postdoctoral grant from Région Ile-De-France.

APPENDIX

A. Relation between the nonlinear susceptibility and molecular orientation:

The electro-optical (EO) effect is the change of the refractive index of a medium in response to a quasi-static electrical field. This effect is related to the second-order nonlinearity and the related EO susceptibility is given by :

$$\boldsymbol{\chi_{ijk}^{(2)}(\omega+\Omega;\omega,\Omega) = Nf^2(\omega)f(\Omega)\iint \beta_{ijk}(\omega+\Omega;\omega,\Omega)P(\breve{\rho})d\breve{\rho}}\ , \quad \textbf{(5)}$$

where $\chi_{ijk}^{(2)}(\omega+\Omega;\omega,\Omega)$ is the nonlinear second-order susceptibility, ω is the optical frequency, Ω is the applied electrical field frequency which can be assumed to be quasi-static compared to that of the optical frequency. N is the density of non-linear chromophores and β is their molecular hyperpolarizability, $\breve{\rho}$ is the solid angle related to the orientation of the molecules, as defined for each molecule by its set of Euler angles. $f(\omega)$ and $f(\Omega)$ are the local field factors at optical frequency and quasi-static frequency. Referring to x,y,z laboratory frame, i,j,k are the macroscopic coordinates. The β tensor of the molecule is known and simple in the axes X,Y,Z associated to the geometry of the molecule. It can be assumed to be one-dimensional, i.e. $\beta = \beta_{zzz}\, z\otimes z\otimes z$, in agreement with the quasi 1-D structure of the dye and related intra-molecular charge transfer that underlies β tensor. The associated coordinates are I,J,K. Taking into account the transformation from X,Y,Z to x,y,z for laboratory axes, Eq. 5 becomes:

$$\boldsymbol{\chi_{ijk}^{(2)}(\omega+\Omega;\omega,\Omega) = Nf^2(\omega)f(\Omega)\sum_{IJK}\iint \beta_{IJK}(\omega+\Omega;\omega,\Omega)P(\breve{\rho})(\hat{I}.\hat{\imath})(\hat{J}.\hat{\jmath})(\hat{K}.\hat{k})d\breve{\rho}}\ . \quad \textbf{(6)}$$

In the case of a bilayer having a thickness e, doped by a nonlinear dye with a surface density N_s we have $N = N_s/e$.

We assume that the molecules are oriented inside the membrane in a cone with a symmetry around the normal z to the membrane surface as shown in Fig. 1 and Fig. 7 , θ_0 being the angle of this cone with respect to the normal.

In the case of a dye oriented inside a membrane in first approximation, one can express the probability of orientation as: $P(\breve{\rho}) = \frac{\delta(\theta-\theta_0)}{2\pi\, sin\theta_0}$, therefore:

$$\boldsymbol{\chi_{ijk}^{(2)}(\omega+\Omega;\omega,\Omega) = \frac{N_s}{e}f^2(\omega)f(\Omega)\beta_{ZZZ}\frac{\iint \delta(\theta-\theta_0)(\hat{I}.\hat{\imath})(\hat{J}.\hat{\jmath})(\hat{K}.\hat{k})d\theta d\varphi}{2\pi}}. \quad \textbf{(7)}$$

This cylindrical symmetry leaves only two independent non-zero coefficients of the $\chi^{(2)}$ tensor, namely:

$$\boldsymbol{\chi_{zzz}^{(2)}} \text{ and } \boldsymbol{\chi_{xxz}^{(2)} = \chi_{yyz}^{(2)} = \chi_{yxy}^{(2)} = \chi_{xzx}^{(2)}} \quad \textbf{(8)}$$

with :

$$\boldsymbol{\chi_{zzz}^{(2)} = \frac{N_s}{e}f^2(\omega)f(\Omega)\beta_{ZZZ}cos^3\theta_0}\ , \quad \textbf{(9)}$$

and

$$\boldsymbol{\chi_{xxz}^{(2)} = \frac{N_s}{e}f^2(\omega)f(\Omega)\beta_{ZZZ}\frac{sin^2\theta_0 cos\theta_0}{2}}\ . \quad \textbf{(10)}$$

Electro-optic coefficients:

The electro-optical coefficients are related to the second-order susceptibility (42), by the relation

$$\boldsymbol{r_{ijk}(\omega) = -\frac{2\chi_{ijk}^{(2)}(\omega+\Omega;\omega,\Omega)}{n_{ii}^2 n_{jj}^2}}\ . \quad \textbf{(11)}$$

We can write those coefficients in the contracted indices mode where ijk will become lk and l stands for a combination of ij (43). It follows the Tab. 2.

From the above geometry and dye characteristics, the electro-optical coefficient tensor matrix of our doped artificial bilayer takes the form:

$$\begin{pmatrix} 0 & 0 & r_{13} \\ 0 & 0 & r_{13} \\ 0 & 0 & r_{33} \\ 0 & r_{13} & 0 \\ r_{13} & 0 & 0 \\ 0 & 0 & 0 \end{pmatrix} , \quad (12)$$

where

$$r_{13} = -\frac{N_s}{en^4} f^2(\omega) f(\Omega) \beta_{ZZZ} sin^2\theta_0 cos\theta_0 , \quad (13)$$

and $$r_{33} = -\frac{N_s}{en^4} f^2(\omega) f(\Omega) \beta_{ZZZ} 2cos^3\theta_0 . \quad (14)$$

These expressions show the dependence of the electro-optical coefficient on the orientation angle θ_0 of the dye. The ration between the two coefficients is directly linked to this angle:

$$\frac{r_{13}}{r_{33}} = \frac{tan(\theta_0)}{2} . \quad (15)$$

EO induced phase shift:

The additional EO phase shift across a membrane of thickness *e*, when the beam is polarized along the $\hat{\imath}$ direction, can be expected as:

$$\Delta\varphi_i = \frac{2\pi}{\lambda} e\Delta n_i , \quad (16)$$

so that :

$$\Delta\varphi_i = -\frac{\pi}{\lambda} e n_i^3 \sum_j r_{ij} E_j , \quad (17)$$

where E_j is the applied quasi-static electric field.

In the configuration where the applied electric field is in the direction normal to the membrane i.e. along z, the only nonzero component of the electrical field is E_3 , then :

$$\Delta\varphi_1 = -\frac{\pi}{\lambda} e n^3 r_{13} E_3 , \quad (18)$$

$$\Delta\varphi_2 = -\frac{\pi}{\lambda} e n^3 r_{13} E_3 , \quad (19)$$

$$\Delta\varphi_3 = -\frac{\pi}{\lambda} e n^3 r_{33} E_3 . \quad (20)$$

B. Case of biological membrane:

In the case of a cell membrane, the surface is not horizontal and the morphology is more complex. The simplest model is a bilayer with a tilt angle α with respect to the horizontal line (see Fig. 8).

In this configuration the new electro-optical coefficients, read in the principal axis system (1',2',3'), can be expressed as a function of the coefficient, in the membrane axis system (1,2,3). They can be written:

$$r_{i',j',k'} = \sum_{i,j,k} r_{i,j,k} (i,i')(j,j')(k,k') \quad (21)$$

In the new axis system the EO coefficient tensor will be then given by:

$$[r'_{ij}] =$$

$$\begin{pmatrix} 0 & r_{13}\sin\alpha & r_{13}\cos\alpha \\ 0 & 3r_{13}\cos^2\alpha\sin\alpha + r_{33}\sin^3\alpha & r_{13}(3\cos^3\alpha - 2\cos\alpha) + r_{33}\sin^2\alpha\cos\alpha \\ 0 & r_{13}(\sin^3\alpha - 2\cos^2\alpha\sin\alpha) + r_{33}\cos^2\alpha\sin\alpha & 3r_{13}\sin^2\alpha\cos\alpha + r_{33}\cos^3\alpha \\ 0 & r_{13}(\cos^3\alpha - 2\sin^2\alpha\cos\alpha) + r_{33}\sin^2\alpha\cos\alpha & r_{13}(\sin^3\alpha - 2\cos^2\alpha\sin\alpha) + r_{33}\cos^2\alpha\sin\alpha \\ r_{13}\cos\alpha & 0 & 0 \\ r_{13}\sin\alpha & 0 & 0 \end{pmatrix} \quad (22)$$

The new phase shift under two perpendicular polarizations can be written:

$$\Delta\boldsymbol{\varphi_{1'}} = \frac{\pi}{\lambda}\frac{N_s f^2(\omega) f^2(\Omega)\beta_{ZZZ}}{en^7}\frac{\sin^2\theta_0\ \cos\theta_0}{\cos\alpha}\boldsymbol{V}, \quad \textbf{(23)}$$

$$\Delta\boldsymbol{\varphi_{2'}} = \frac{\pi}{\lambda}\frac{N_s f^2(\omega) f^2(\Omega)\beta_{ZZZ}}{en^7}\frac{\cos^2\alpha\sin^2\theta_0\ \cos\theta_0+2\cos^3\theta_0\sin^2\alpha}{\cos\alpha}\boldsymbol{V}. \quad \textbf{(24)}$$

A dependency on the tilt angle is clearly expected.

C. Homodyne and synchronous detection:

If a reference beam of amplitude $\bar{\alpha}_{LO}$ is interfering with a signal beam of amplitude $\bar{\alpha}_S$, the difference in the intensities detected by the two photodiodes used in balanced homodyne detection configuration is:

$$\Delta\boldsymbol{I} = \boldsymbol{2\bar{\alpha}_{LO}\bar{\alpha}_S\cos(\Delta\varphi - \varphi_{OL})} \quad \textbf{(25)}$$

where φ_{OL} is the static optical phase-shift between the two beams paths, and $\Delta\varphi$ the electro-optical phase-shift in the signal path. While we are interested in measuring $\Delta\varphi$ one can wonder whether a signal amplitude variation due to absorption or emission $\Delta\bar{\alpha}_S$ could contribute to the signal.

Two regimes are of interest depending on the static phase shift value.
First, if $\varphi_{OL} = \pi/2$, eq. 25 became $\Delta I \approx 2\bar{\alpha}_{LO}\bar{\alpha}_S\Delta\varphi$, provided that the electro-optical phase shift $\Delta\varphi$ is small. The electric field being modulated at a frequency Ω, the EO phase shift will be modulated at the same frequency ($\Delta\varphi = \varphi_0\cos(\Omega t + \theta_1)$) as well as the emission or absorption $\bar{\alpha}_S = \bar{\alpha}_S + \Delta\bar{\alpha}_S(\Omega) = \bar{\alpha}_S + \bar{\alpha}_{S0}\cos(\Omega t + \theta_2)$.Then

$$\boldsymbol{\Delta I = 2\bar{\alpha}_{OL}\bar{\alpha}_S\varphi_0\cos(\Omega t + \theta_1) + \bar{\alpha}_{OL}\bar{\alpha}_{S0}\varphi_0(\cos(\theta_1 - \theta_2) + \cos(2\Omega t + \theta_1 + \theta_2))}. \quad \textbf{(26)}$$

The synchronous detection multiplies ΔI by a reference signal at the electric field frequency Ω. After such multiplication the DC component carries the information of the EO phase shift corresponding to the first term in equation (26) $\bar{\alpha}_{OL}\bar{\alpha}_S\varphi_0$. The two last components are shifted spectrally to higher frequency, which includes the intensity variation $\Delta\bar{\alpha}_S$ due to absorption or emission variation. Therefore $\Delta\bar{\alpha}_S$ will not show-up in the DC expression.

Second, if $\varphi_{OL} = 0$; then the intensity difference becomes $\Delta I = 2\bar{\alpha}_{LO}\bar{\alpha}_S\cos(\Delta\varphi) \approx 2\bar{\alpha}_{LO}\bar{\alpha}_S$ if $\Delta\varphi$ is very small. In this case any variation in the amplitude of the signal due to absorption or emission induced by electric field and modulated with the same frequency will be measured with the lock-in amplifier.

Therefore an interesting feature of our method is to be able to access either EO coefficient or electric field-induced absorption and emission variation, depending on the phase shift φ_{OL} that we impose between the two interfering beams we can.

, , .

References:

1. Hodgkin, A. L. and A. F. Huxley. 1939. Action potentials recorded from inside a nerve fibre. Nature 144:710-711.

2. Llinas, R. and M. Sugimori. 1980. Electrophysiological properties of in vitro Purkinje cell somata in mammalian cerebellar slices. J Physiol 305:171-195.

3. Sakmann, B. and N. E. 1984. Patch Clamp Techniques for Studying Ionic Channels in Excitable-Membranes. Annual Review of Physiology 46:455-472.

4. Cohen, L. B., R. D. Keynes, and B. Hille. 1968. Light scattering and birefringence changes during nerve activity. Nature 218:438-441.

5. Cohen, L. B., B. Hille, and R. D. Keynes. 1970. Changes in axon birefringence during the action potential. J Physiol 211:495-515.

6. Gupta, R. K., B. M. Salzberg, A. Grinvald, L. B. Cohen, K. Kamino, S. Lesher, M. B. Boyle, A. S. Waggoner, and C. H. Wang. 1981. Improvements in optical methods for measuring rapid changes in membrane potential. J Membr Biol 58:123-137.

7. Cohen, L. B., B. M. Salzberg, and A. Grinvald. 1978. Optical methods for monitoring neuron activity. Annu Rev Neurosci 1:171-182.

8. Ross, W. N., B. M. Salzberg, L. B. Cohen, A. Grinvald, H. V. Davila, A. S. Waggoner, and C. H. Wang. 1977. Changes in absorption, fluorescence, dichroism, and Birefringence in stained giant axons: : optical measurement of membrane potential. J Membr Biol 33:141-183.

9. Loew, L. M. 1996. Potentiometric dyes: Imaging electrical activity of cell membranes. Pure and Applied Chemistry 68:1405-1409.

10. Zochowski, M., M. Wachowiak, C. X. Falk, L. B. Cohen, Y. W. Lam, S. Antic, and D. Zecevic. 2000. Imaging membrane potential with voltage-sensitive dyes. Biol Bull 198:1-21.

11. Zecevic, D. 1996. Multiple spike-initiation zones in single neurons revealed by voltage-sensitive dyes. Nature 381:322-325.

12. Gross, E., R. S. Bedlack, and L. M. Loew. 1994. Dual-Wavelength Ratiometric Fluorescence Measurement of the Membrane Dipole Potential. Biophys J 67:208-216.

13. Dombeck, D. A., M. Blanchard-Desce, and W. W. Webb. 2004. Optical recording of action potentials with second-harmonic generation microscopy. J Neurosci 24:999-1003.

14. Bouevitch, O., A. Lewis, I. Pinevsky, J. P. Wuskell, and L. M. Loew. 1993. Probing Membrane-Potential with Nonlinear Optics. Biophys J 65:672-679.

15. Moreaux, L., T. Pons, V. Dambrin, M. Blanchard-Desce, and J. Mertz. 2003. Electro-optic response of second-harmonic generation membrane potential sensors. Opt Lett 28:625-627.

16. Toury, T., S. Brasselet, and J. Zyss. 2006. Electro-optical microscopy: mapping nonlinear polymer films with micrometric resolution. Opt Lett 31:1468-1470.

17. Pons, T., L. Moreaux, O. Mongin, M. Blanchard-Desce, and J. Mertz. 2003. Mechanisms of membrane potential sensing with second-harmonic generation microscopy. Journal of Biomedical Optics 8:428-431.

18. Boyd, R. W. 2008. Nonlinear Optics: Academic Press.

19. Born, M. and E. Wolf. 1999. Principles of Optics - Electromagnetic Theory of Propagation, Interference and Diffraction of Light. m. F.-B. a. E. Wolf, editor. Cambridge: Cambridge University Press.

20. Le Xuan, L., S. Brasselet, F. Treussart, J. F. Roch, F. Marquier, D. Chauvat, S. Perruchas, C. Tard, and T. Gacoin. 2006. Balanced homodyne detection of second-harmonic generation from isolated subwavelength emitters. Appl Phys Lett 89.

21. Suzuki, H., B. Le Pioufle, and S. Takeuhci. 2008. Ninety-six-well planar lipid bilayer chip for ion channel recording fabricated by hybrid stereolithography. Biomed Microdevices.

22. Le Pioufle, B., H. Suzuki, K. V. Tabata, H. Noji, and S. Takeuchi. 2008. Lipid bilayer microarray for parallel recording of transmembrane ion currents. Analytical Chemistry 80:328-332.

23. Suzuki, H., K. V. Tabata, H. Noji, and S. Takeuchi. 2006. Highly reproducible method of planar lipid bilayer reconstitution in polymethyl methacrylate microfluidic chip. Langmuir 22:1937-1942.

24. Ide, T. and T. Ichikawa. 2005. A novel method for artificial lipid-bilayer formation. Biosensors & Bioelectronics 21:672-677.

25. Rohr, S. and B. M. Salzberg. 1994. Multiple-site optical-recording of transmembrane voltage (Msortv) in patterned growth heart cell-cultures - assessing electrical behavior, with microsecond resolution, on a cellular and subcellular scale. Biophys J 67:1301-1315.

26. Bullen, A. and P. Saggau. 1999. High-speed, random-access fluorescence microscopy: II. Fast quantitative measurements with voltage-sensitive dyes. Biophys J 76:2272-2287.

27. Ries, R. S., H. Choi, R. Blunck, F. Bezanilla, and J. R. Heath. 2004. Black lipid membranes: visualizing the structure, dynamics, and substrate dependence of membranes. Journal of Physical Chemistry B 108:16040-16049.

28. Antic, S. and D. Zecevic. 1995. Optical signals from neurons with internally applied voltage-sensitive dyes. J Neurosci 15:1392-1405.

29. Clarke, R. J. 1997. Effect of lipid structure on the dipole potential of phosphatidylcholine bilayers. Biochimica Et Biophysica Acta-Biomembranes 1327:269-278.

30. Clarke, R. J. and D. J. Kane. 1997. Optical detection of membrane dipole potential: Avoidance of fluidity and dye-induced effects. Biochimica Et Biophysica Acta-Biomembranes 1323:223-239.

31. Shynkar, V. V., A. S. Klymchenko, G. Duportail, A. P. Demchenko, and Y. Mely. 2005. Two-color fluorescent probes for imaging the dipole potential of cell plasma membranes. Biochimica Et Biophysica Acta-Biomembranes 1712:128-136.

32. Zhang, J., R. M. Davidson, M. D. Wei, and L. M. Loew. 1998. Membrane electric properties by combined patch clamp and fluorescence ratio imaging in single neurons. Biophys J 74:48-53.

33. Lambacher, A. and P. Fromherz. 2001. Orientation of hemicyanine dye in lipid membrane measured by fluorescence interferometry on a silicon chip. Journal of Physical Chemistry B 105:343-346.

34. Fujiwara, H., M. Fujihara, and T. Ishiwata. 2003. Dynamics of the spontaneous formation of a planar phospholipid bilayer: A new approach by simultaneous electrical and optical measurements. Journal of Chemical Physics 119:6768-6775.

35. Hall, J. E. 1975. Access resistance of a small circular pore. J Gen Physiol 66:531-532.

36. Lis, L. J., M. Mcalister, N. Fuller, R. P. Rand, and V. A. Parsegian. 1982. Interactions between neutral phospholipid-bilayer membranes. Biophys J 37:657-665.

37. Crowley, J. M. 1973. Electrical breakdown of biomolecular lipid-membranes as an electromechanical instability. Biophys J 13:711-724.

38. Kramar, P., D. Miklavcic, and A. M. Lebar. 2007. Determination of the lipid bilayer breakdown voltage by means of linear rising signal. Bioelectrochemistry 70:23-27.

39. Lebar, A. M., G. C. Troiano, L. Tung, and D. Miklavcic. 2002. Inter-pulse interval between rectangular voltage pulses affects electroporation threshold of artificial lipid bilayers. IEEE Trans Nanobioscience 1:116-120.

40. Dorn, R., S. Quabis, and G. Leuchs. 2003. Sharper focus for a radially polarized light beam. Physical Review Letters 91.

41. Agrawal, G. P. Fiber-Optic Communication Systems.

42. Sigelle, M. and R. Hierle. 1981. Determination of the electrooptic coefficients of 3-methyl 4-nitropyridine 1-oxide by an interferometric phase-modulation technique. Journal of Applied Physics 52:4199-4204.

43. Yariv, A. and P. Yeh. 2003. Optical Waves in Crystals - propagation and control of laser radiation. W. C. Library, editor. New Jersey: John Wiley & Sons, Inc., Hoboken.

	EO phase shift ($\times 10^{-4}$rad)	
Polarization of the light	Artificial membrane	$LiNbO_3$ crystal
x	2.09 ± 0.14	1.82 ± 0.15
y	2.12 ± 0.23	20.12 ± 2.32

Tab. 1: Table showing the measured EO phase shift in radiant for two perpendicular light polarizations passing through the sample: (left) in the case of an artificial membrane the EO phase shift is the same for both polarizations (5 volts at 20 kHz) within error , and (right) in the case of a reference sample made of a $LiNbO_3$ crystalline plate the ratio between the two signals is around 10 (modulation of 10 volts at 20kHz).

ij	xx = 11	yy = 22	zz = 33	yz = 23	xz = 13	xy = 12
l	1	2	3	4	5	6

Tab. 2: Table of contracted indices.

Fig. 1 : Principle of probing the electro-optical effect of a one-side dye-doped membrane. Inset: orientation distribution of the dye molecules in the upper layer.

Fig. 2: Simplified scheme of the interferometric microscope used to detect the electro-optical phase shift associated to the dye-doped membrane. S: cw HeNe laser source – O: microscope objective (40×, N.A. 0.6) – P: photodiode – G: high frequency voltage generator – L: lock-in amplifier.

Fig. 3: Steps of bilayer formation: (a) insertion of the buffer and the dye in the upper channel, (b) injection of the lipid in the lower channel, (c) injection of the buffer solution in the lower channel and formation of the bilayer.

Fig. 4: Electro-optical temporal response of the bilayer without any modulating field, then while applying a difference of potential of amplitude 5V modulated at 20 kHz frequency. The signal-to-noise ratio is around 10±1 for 20ms integration time.

Fig. 5: EO phase shift vs applied modulated voltage amplitude

Fig. 6 : A scan image of the EO response of dye-doped bilayer. Inset: destruction of the bilayer during a scan.

Fig. 7 : Molecule orientation with respect to the coordinate axis.

Fig. 8: Scheme of axes configuration in case of a tilted membrane

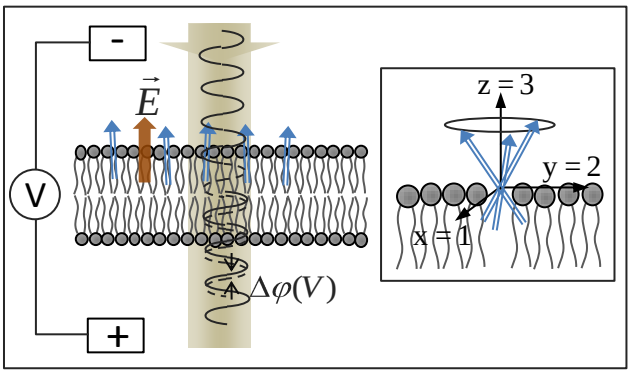

Fig. 1

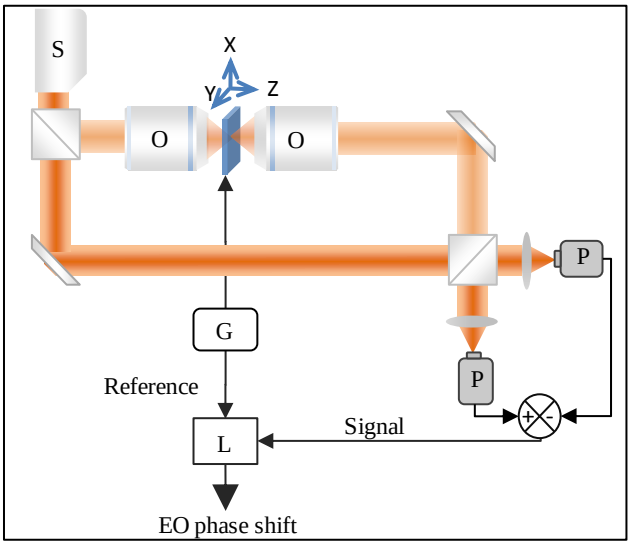

Fig. 2

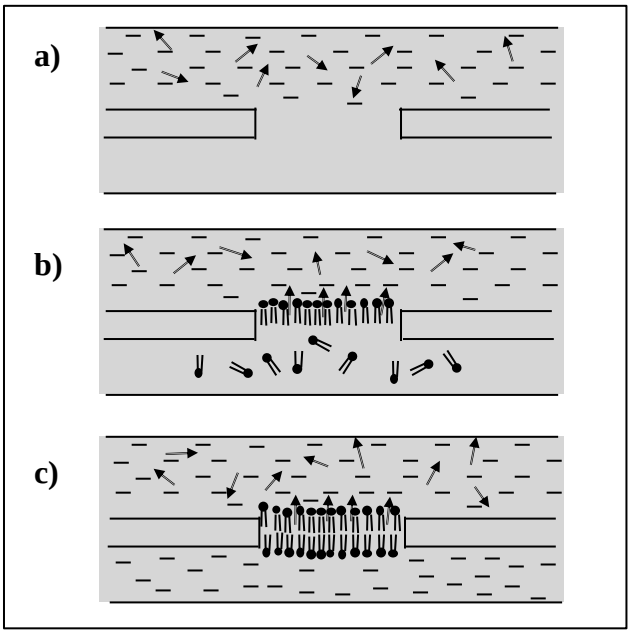

Fig. 3

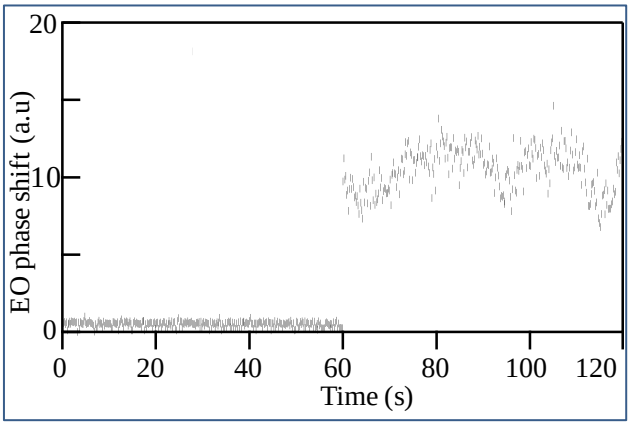

Fig. 4

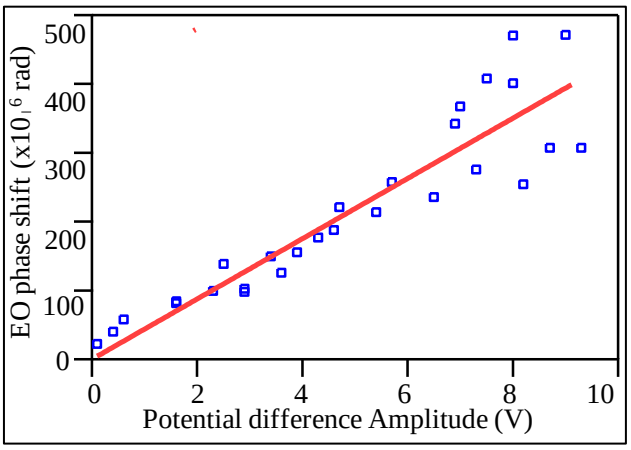
EO phase shift (x10^{-6} rad)
500
400
300
200
100
0
0
2
4
6
8
10
Potential difference Amplitude (V)

Fig. 5

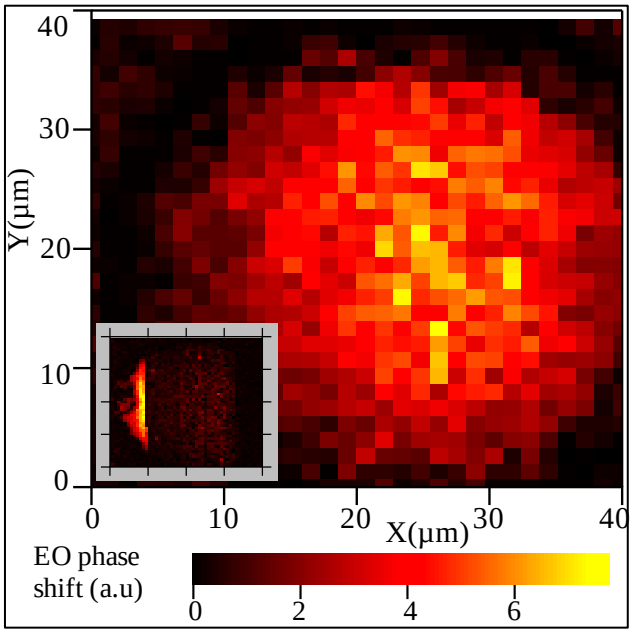

Fig. 6

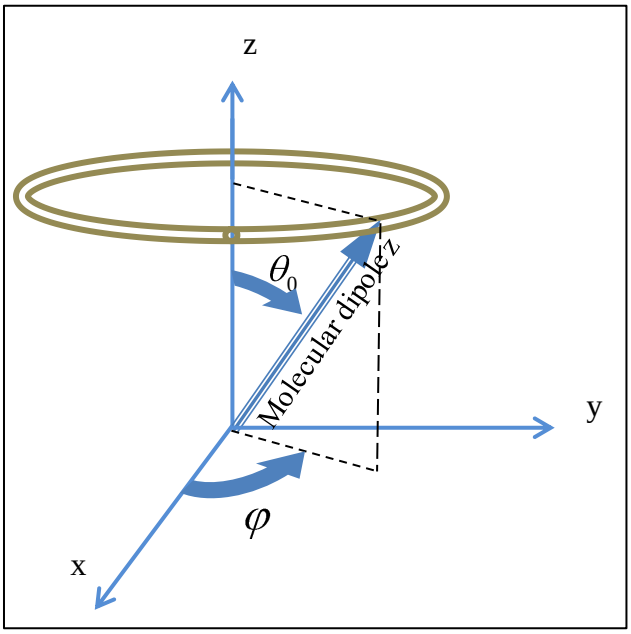

Fig. 7

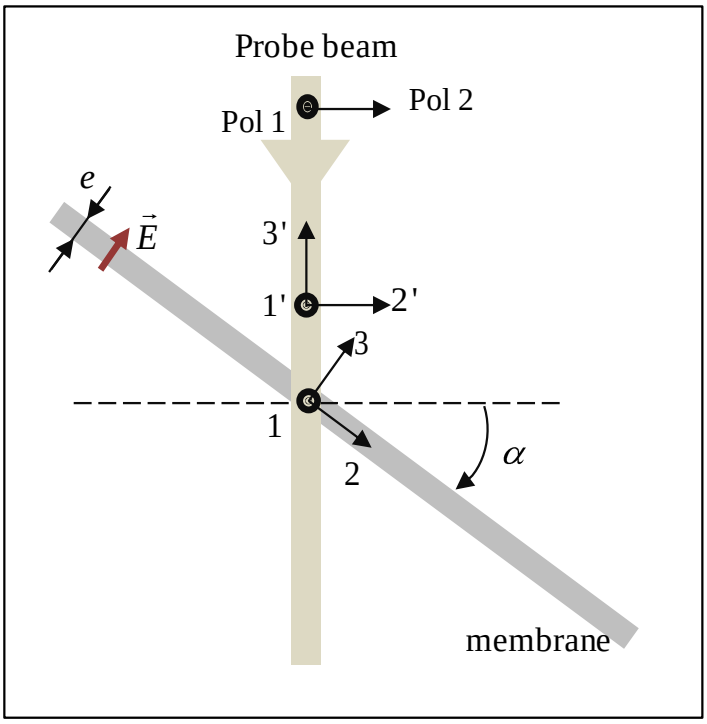

Fig. 8